Available online at www.sciencedirect.com

SciVerse ScienceDirect

Procedia IUTAM 3 (2012) 205 – 227

Procedia IUTAM

www.elsevier.com/locate/procedia

Microstructure to Macro-Scale Using Gradient Plasticity with Temperature and Rate Dependent Length Scale

George Z. Voyiadjis[a,*], Danial Faghihi[a]

[a]*Department of Civil and Environmental Engineering, Louisiana State University, Baton Rouge, LA 70803, USA*

Abstract

Gradient plasticity theory formulates a constitutive framework on the continuum level that bridges the gap between the micromechanical plasticity and classical continuum plasticity by incorporating the material length scale. A micromechanical-based model of variable material intrinsic length scale is developed in the present work which allows for variations in temperature and strain rate and its dependence on the grain size and accumulated plastic strain. The material constants of the proposed model are calibrated using the size effect encounter in nanohardness experiments. In this regard, two different physically based models for Temperature and Rate Indentation Size Effects (TRISE) are also developed in this work for single and polycrystalline metals by considering different expressions of the geometrical necessary dislocation (GND) density. The results of indentation experiments performed on various single- and polycrystalline materials are then used here to implement the aforementioned framework in order to predict simultaneously the TRISE and variable length scale at different temperatures, strain rates and various grain sizes.

Keywords: Gradient plasticity; Length scale; size effect; nanoindentation

1. Introduction

The size dependency of mechanical properties of metallic materials such as flow stress or hardness has been widely proven in the literature [1]. Since classical continuum plasticity does not incorporate material length scales, it is not able to predict the size dependency. However, strain gradient plasticity [2-4] is successful in explaining such size effects encountered in many micro- and nano- advanced technologies. These theories are proposed based on introducing a gradient in the constitutive relationships to account for the micro-structural interaction where the material behavior at any point is assumed to depend not only on the state of that point but also on the state of its eighboring region by proposing the representative length scale ℓ of the deformation field to set the qualitative

*Corresponding author. Tel: +1-225-578-8668; fax: +1-225-578-8662
Email address: voyiadjis@eng.lsu.edu (George Z. Voyiadjis)
URL: http://www.csmlab.lsu.edu (George Z. Voyiadjis)

2210-9838 doi:10.1016/j.piutam.2012.03.014

and quantitative behavior of size effects. In this way, the gradient theories bridge the gap between the macro and micro/nano-scale and it gives reasonable agreements with size dependence of mechanical behavior at small scales as well as the determination of the widths of shear bands, and dispensed with the mesh dependence of finite element calculations in the material softening regime. The main issue in strain gradient plasticity is the determination of the material intrinsic length scale that scales with strain gradient using the stress-strain behavior from macroscopic tests along with information from micromechanical tests. It is known that indentation experiments (nano/micro) may be the most effective tests for measuring the length scale parameter ℓ[5]. In this work, an attempt is made to determine this parameter through nanoindentation experiments. Using the gradient theory and crystal plasticity, an expression that describes the hardness as a function of indentation depth can be derived. Combining this expression with the outcomes of nanoindentation experiments of a material allows one to determine the value of the material intrinsic length scale ℓ. It is known that the polycrystalline materials, hardness always decreases with increasing grain size due to lower dislocation densities. The possibility of measuring an intrinsic hardening contribution of the grain boundary, as a result of the difficulty in slip transmission across the boundary, has recently come under investigation with the widespread availability of the nanoindentation technique. Low-load indentation experiments [6, 7] have shown significant hardening effects within a distance of the order of 1 μm from the boundary. Such experiments could potentially offer detailed information about the intrinsic mechanical properties of individual grain boundaries. Contrary to classical nanoindentation experiments which show that the hardness decreases with increase in indentation depth, recent experiments have shown that, at small nanometer depths from the surface [8-15], some metals experience a local increase in hardness with increase in indentation depth. Based on the indentation load and depth at which these excursions are observed, it was proposed that they are certain bursts due to dislocation pile up and subsequent transmission across the boundary. That is, in this new type of size effect, which termed as hardening/softening behavior here, the hardness at which the excursion takes place increases as the indenter tip to boundary distance decreases. Moreover, hardness is known to be sensitive to strain rate and temperature. On the micro-scale level, strain rate is known to be related to the dislocation density and average dislocation velocity through the Orowan equation [16]. In addition, flow stress can be related to dislocation density using the Taylor hardening law [17]. Hardness also decreases with increasing temperature for bulk metals, single crystals and thin films [18]. In this work, a physically based model with Temperature and Rate Indentation Size Effects (TRISE) for single and polycrystalline metals is derived. This model is also able to capture the hardening/softening effect encountered in polycrystalline materials by considering the effect of the grain boundary. Moreover, the variable material length scale parameter ℓ for gradient isotropic hardening plasticity is identified through calibrating the physically based model of the length scale using nanoindentation experiments. The proposed models are investigated in order to capture the behavior of the FCC and BCC materials for different grain sizes (or the distance of indenter from grain boundary in the coarse grained metals), accumulated plastic strains, rates of strain and various temperatures. Results from nanoindentation experiments on different FCC and BCC metals are used to evaluate the proposed length scale. Furthermore, a method for identifying the material length scale parameters from indentation tests is presented, and the variable length scale of the above mentioned materials is obtained.

2. Physical Interpretation of Length Scales

Gradient plasticity is introduced through the non-local weak form of the conventional effective plastic strain. In general, the non-local form ($\hat{p}$) is written in terms of its local counterpart (p) and high order gradient terms [19] as follows:

$$\hat{p} = [p^{\gamma} + (\ell\eta)^{\gamma}]^{1/\gamma} \tag{1}$$

Where ℓ is the length scale parameter that is required for dimensional consistency,η is the effective plastic strain gradient of any order and γ is an interaction coefficient. The flow stress (σ) can be written at the macroscopic level using a power law ($\sigma = k\hat{p}^{1/m}$), and combining this with Eq. (1) yields:

$$\sigma = k[p^{\gamma} + \ell^{\gamma}\eta^{\gamma}]^{1/m\gamma} \tag{2}$$

where k and m are material constants. One method to enhance the coupling between statistically stored dislocation (SSDs) and geometrically necessary dislocation (GNDs) at the microscopic level is to assume that the overall shear flow stress, τ_f , has two components: one arising from SSDs, τ_s , and another component due to GNDs, τ_G. Ashby

[20] has pointed out that, in general, the presence of GNDs will accelerate the rate of SSDs storage and that an arithmetic sum of their densities, as considered by Nix and Gao [21], gives a lower limit on total dislocation density (ρ_T), so that a higher total dislocation density can be obtained. The following general functional form for τ_f is then chosen as follows in the spirit of Eq. (2) [22]:

$$\tau_f = [\tau_S^\beta + \tau_G^\beta]^{1/\beta} \tag{3}$$

where β is considered as a material constant, termed the interaction coefficient, and used to assess the sensitivity of predictions to the way in which the coupling between SSDs and GNDs is enhanced during the plastic deformation process. Using Eqs. (3) along with Taylor's hardening law for τ_S and τ_G, the overall flow stress at the micro scale can be obtained as follows:

$$\tau_f = \alpha_S G b_S \sqrt{\rho_T} \text{ with } \rho_T = [\rho_S^{\beta/2} + (\alpha_G^2 b_G^2 \rho_G / \alpha_G^2 b_G^2)^{\beta/2}]^{2/\beta} \tag{4}$$

where, b_S and b_G are the magnitudes of the Burgers vector for SSDs and GNDs respectively, G is the shear modulus, ρ_S and ρ_G denote the density of SSDs and GNDs respectively, ρ_T is total dislocation density, and α_S and α_G are the statistical coefficients which account for the deviation from regular spatial arrangements of the SSDs and GNDs populations respectively. A number of authors showed that the gradient in the plastic strain field is accommodated by the GND density ρ_G such that the effective strain gradient η introduced in Eq.(1) is defined as [23]:

$$\eta = \rho_G b_G / \bar{r} \tag{5}$$

where $\bar{r}$ is the Nye factor introduced by Arsenlis and Parks [23] to reflect the scalar measure of GND density resultant from macroscopic plastic strain gradients . Gao et al. [24] indicated that the Nye factor is an important parameter in the predictions of the gradient plasticity theories as compared to the experimental results. The plastic shear strain γ^p can be defined as a function of the SSD density ρ_S as follows [25]:

$$\gamma^p = b_S L_S \rho_s \tag{6}$$

where L_s is the mean spacing between SSDs. Using Schmidt's orientation tensor, M_{ij} , to link the plastic strain in micro and macro scales and deriving the expressions for ρ_S and ρ_G as a function of the effective plastic strain p and the effective plastic strain gradient η respectively, and substituting them in Eqs.(4), yields an expression for τ.Combining this expression with $\sigma = Z\tau$ (Taylor law [17]) finally yields the flow stress in microscopic level:

$$\sigma = \alpha_S G Z \sqrt{b_S / L_S M}[p^{\beta/2} + (\alpha_G^2 b_G L_S M \bar{r} / \alpha_S^2 b_S)^{\beta/2} \eta^{\beta/2}]^{1/\beta} \tag{7}$$

In Eq. (7), M is the Schmidt factor and Z is a constant that varies depending on the material type. The Taylor factor Z acts as an isotropic interpretation of the crystalline anisotropy at the continuum level [24]. Comparing Eqs. (2) corresponding to macro and (7) corresponding to micro flow stress yields the following expression for the material length scale which bridge the gap between the two scales:

$$\ell = (\alpha_G / \alpha_S)^2 (b_G / b_S) L_S M \bar{r} \tag{8}$$

In order to account for its rate and temperature dependency, the equation for L_S proposed by Gracio [26] is modified by Voyiadjis and his co-workers [15, 27-29] for single and polycrystalline materials as a function of temperature (T) and the equivalent plastic strain rate ($\dot{p}$). Substituting these expressions into Eq. (8), the following physics-based equations for the material length scale of single- and polycrystalline materials will be obtained respectively:

$$\ell = (\alpha_G / \alpha_S)^2 (b_G / b_S) M \bar{r} \left(\frac{\delta_1 e^{-(E_r / R_g T)}}{(1 + \delta_2 p^{(1/m)})(1 + \delta_3 \dot{p}^q)} \right) \tag{9}$$

$$\ell = (\alpha_G / \alpha_S)^2 (b_G / b_S) M \bar{r} \left(\frac{\delta_1 d e^{-(E_r / R_g T)}}{(1 + \delta_2 d p^{(1/m)})(1 + \delta_3 \dot{p}^q)} \right) \tag{10}$$

Where R_g is the gas constant,E_r is the activation energy (energy per mole), m is hardening exponent corresponding to strain, d is the grain size and δ_1, δ_2, and δ_3 in the above equations are material constants which can be obtained using nanoindentation tests and which will be explained in the next section.

3. Model for Temperature and Rate Indentation Size Effect (TRISE)

Following the Nix and Gao's [21] approach in considering the generation of GNDs under the indenter during hardness experiments, Voyiadjis and Abu Al-Rub [30] derived a more general framework of equations that can be used to identify the material intrinsic length scale parameter using micro-hardness results of spherical and pyramidal indenters. They proposed the following relation for micro hardness:

$$H = Z\kappa\alpha_S G b_S [\rho_S^{\beta/2} + (\alpha_G b_G/\alpha_S b_S)^{\beta}\rho_S^{\beta/2}]^{1/\beta} \tag{11}$$

They also defined the macro-hardness H_0 as the hardness experienced at greater indentation depths, where there are no size effects in the absence of the strain gradient (and thus GNDs) using the following equation:

$$H_0 = Z\kappa\tau_S = Z\kappa\alpha_S G b_S \sqrt{\rho}_S \tag{12}$$

Making use of Eqs. (11) and (12) and simplifying the result under the assumption that $\alpha_S = \alpha_G$ and $b_S = b_G$ yields the following hardness ratio:

$$\left(\frac{H}{H_0}\right)^{\beta} = 1 + \left(\frac{\rho_G}{\rho_S}\right)^{\beta/2} \tag{13}$$

By considering of Eqs.(6), (8) and Tabor [31] relation for mapping from the hardness-indentation depth curve to the tensile stress-plastic curve (i.e. $H = \kappa\sigma_f$), the expression of ρ_S for conical indenter can be obtained as follows:

$$\rho_S = \frac{c\bar{r}\alpha_G^2 b_G \tan\theta}{\ell b_S^2 \alpha_S^2} \tag{14}$$

where c is a material constant with a value of $c = 0.4$. The difference between single- and poly-crystal TRISE comes to the formulation as a result of the various expression of the ρ_G. The expression of the GND density for single crystals is obtained based on the approach of Nix and Gao [21] in the generation of GNDs under the indentation as follow:

$$\rho_G = \frac{3\tan^2\theta}{2b_G h} \tag{15}$$

where in both expressions of GND and SSD densities θ is the angle between the surface of the conical indenter and the plane of the surface. Substituting these equations into Eq. (13) along with the Eq. (9) and the assumption of $\alpha_S = \alpha_G$ and $b_S = b_G$, the TRISE for single crystal materials is obtained as follows:

$$H = H_0\left[1 + \left[\frac{3M\tan\theta}{2c(h-h^*)}\left(\frac{\delta_1 e^{-(E_r/R_g T)}}{(1+\delta_2 p^{(1/m)})(1+\delta_3 \dot{p}^q)}\right)\right]^{\beta/2}\right]^{1/\beta} \tag{16}$$

where h^* in this equation is a material parameter. However, In the case of polycrystalline materials, the hardening/softening effect needs to be included through the concept of the plastic zone beneath the indenter which is explained by many researchers (e.g [7]) and formulated by Yang and Vehoff [9] and Faghihi and Voyiadjis [28]. Voyiadjis and co-workers (e.g. [11,29]) identified three regions where the TRISE of the hardness changes as shown in Figure 1(b). They referred to Regions I and III, where the hardness decreases with increasing depth, as being dominated by the strain gradient plasticity mechanism. They also concluded that Region II was dominated by grain boundaries acting as barriers to dislocation movement resulting in an increase in hardness with increasing depth. The hardening effect is driven by the volume of the plastic zone beneath the indenter increasing in size until it is obstructed by the grain boundaries. However, as the loading increases, more GNDs are pushed into the pile-up, and its length is reduced as the indent grows, leading to an increasing stress concentration at the head of the pile up. Eventually, the shear stress on the slip system in the next grain is sufficiently high to activate a dislocation source near or on the grain boundary. Dislocations move away rapidly, causing the observed softening. This plastic deformation relieves the back stress that had been generated by the blocked dislocation pile-up and leads to a release of energy, which is seen as an increment in the indentation penetration at near constant load in load-depth curve (Figure 1(a)).

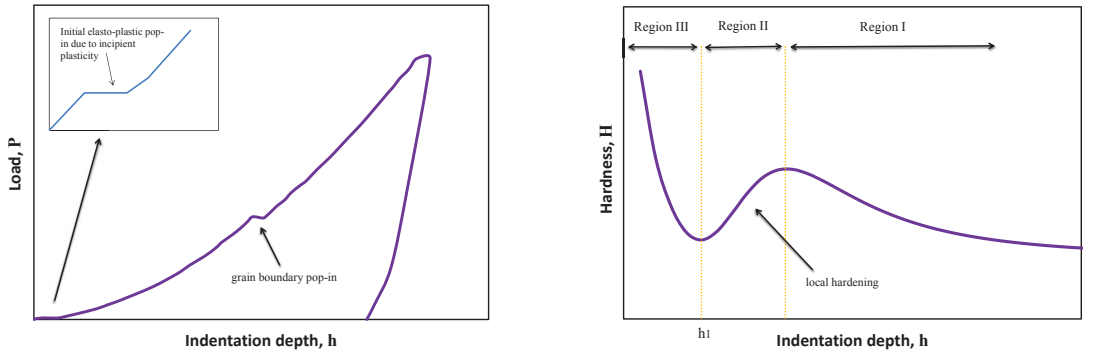

(a) (b)

Fig. 1: (a) Load-displacement curve showing the grain boundary pop-in; (b) Typical hardness-displacement curve showing the hardening/softening effect.

In the release of the pile-ups into the adjacent grain, several mechanisms may be active, including direct transmission across the boundary (for screw components if the slip planes in both grains intersect the boundary in a common line), absorption by dissociation in the boundary, and dislocation absorption and subsequent re-emission [32]. The proposed mechanism of dislocation absorption and re-emission is supported by in situ transmission electron microscopy studies of slip propagation across boundaries in BCC metals [33] which is visualized in Figure 2. In some cases, dislocations were found to stop at a short distance from the grain boundary and cross-slip into a plane nearly parallel to the boundary [34]. The aforementioned phenomenon has been included into the formulation based on the work of Yang and Vehoff [9] which lead to the following expression of GNDs density for polycrystalline materials:

$$\rho_G = \frac{\lambda}{V_{plastic}} = \frac{\frac{\pi}{b_G}\frac{h^2}{\tan\theta}}{\delta_4 \frac{\pi}{12} d^3 - 8.19h^3} \tag{17}$$

where λ is the total length of the injected GND loop and $V_{plastic}$ is the volume of the plastic region under the indenter. Making use of this result for ρ_G and the variable material length scale leads to the following expressions for the hardness in polycrystalline materials:

$$H = H_0(1 + C(h))\left[1 + \left[\frac{M\pi(h - h^*)^2}{\left(\delta_4 \frac{\pi}{12} d^3 - 8.19(h - h^*)^3\right) c \tan^2\theta}\left(\frac{\delta_1 d e^{-(E_r/R_g T)}}{(1 + \delta_2 d p^{(1/m)})(1 + \delta_3 \dot{p}^q)}\right)^{\beta/2}\right]^{1/\beta}\right] \tag{18}$$

where δ_1, δ_2,δ_3, and δ_4 are material parameters that are determined experimentally. Furthermore, $(1 + C(h))$ is included in the model so as to use the cyclic plasticity model developed by Voyiadjis and Abu Al-Rub [35] and Voyiadjis and Basuroychowdhury [36], where $C(h) = \sqrt{1/h}$. The material constants δ_1, δ_2,δ_3, and δ_4 can be obtained by fitting Eqs. (16) and (18) through the nanoindentation test results. Once these constants are calibrated experimentally, the material length scales can be obtained using Eqs. (9) and (10).

In order to make the aformationed fitting, an expression for the macro hardness (H_0) is required as well as the variation of the equivalent plastic strain (p) as a function of the indentation depth. Also a relation between the material parameter h^* and grain size (d) needs to be determined. The relations and the approaches used for finding these parameters are explained in the following:

- By using the expression of the ratio of the effective radius to the contact radius suggested by Feng and Nix [37], Faghihi and Voyiadjis [28] suggested the following relation between the grain size and the parameter h^*:

$$d = 4.35h^*(1 + \delta_5 e^{-h^*/\delta_6}) \tag{19}$$

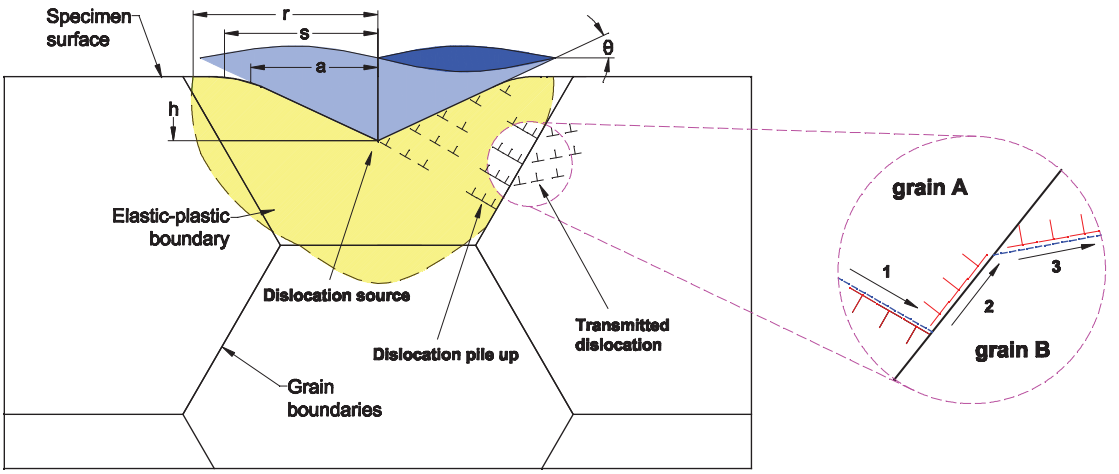

Fig. 2: The expansion of the plastic zone, GNDs pile up near grain boundary and transmission of dislocations across a grain boundary through dislocation absorption and re-emission mechanism.

where δ_5 and δ_5 are fitting parameters. Using this equation and knowing δ_5 and δ_5 , the value of h^* can be obtained from the grain size.

- In order to find the value of H_0 for different temperatures and strain rates, the physically based model based on dislocation mechanisms developed by Almasri and Voyiadjis [38] is taken into account. According to this model the hardness behavior is divided into two regions: (a) at low strain rate ($\dot{\epsilon} \leqslant 10^3/s$) the hardness (and the flow stress) is governed by the thermally activated mechanism; (b) at high strain rates the rates of viscous drag mechanism becomes the main mechanism and the hardness increases rapidly with increasing strain rate. This model is as follows [38]:

$$H_0 = \begin{cases} \frac{\kappa Z}{lb^2}\left(U_0 - KT\ln\left(\frac{\dot{\varepsilon}}{MNl^2b\nu}\right)\right) & \frac{H_0 b}{\nu\kappa\, ZlB} e^{\left(\frac{U_0}{KT} - \frac{lb^2 H_0}{\kappa ZKT}\right)} \gg 1 \\ \frac{\kappa ZB}{MNlb^2}\dot{\varepsilon} & \frac{H_0 b}{\nu\kappa\, ZlB} e^{\left(\frac{U_0}{KT} - \frac{lb^2 H_0}{\kappa ZKT}\right)} \ll 1 \end{cases} \tag{20}$$

where N is the number of the mobile segments per unit volume, l is the mean distance between the forest dislocations,U_0 is the energy required to form a jog ($U_0 = Gb^3/2$),ν is the frequency factor, K is the Boltzmann constant, B is the dislocation drag coefficient, T is the absolute temperature, M is the Schmidt factor [39], and Z and κ are the Taylor factor ($\sigma_f = Z\tau_f$) [17] and the Tabor factor ($H = \kappa\sigma_f$) [31] respectively. The term Nl also characterizes the total length of the moving segments per unit volume or density of moving dislocations.

- " The amount of the equivalent plastic strain as a function of the indentation depth ($p = p(h)$) is obtained using a finite element analysis of the indentation problem. In this regard, the physically based viscoplastic constitutive relation for BCC and FCC metals proposed by Voyiadjis and Abed [40, 41] are taken into account. These models are developed within the framework of additive decomposition of thermal and athermal yield stress and based on thermal activation analysis as well as dislocation interaction mechanisms. The physically based thermal/dynamic yield function is used in deriving the evolution of the governing equations. The dynamic flow rule for the different materials are as follows:

$$f_d^{th} = \sigma_{eq} - Y_a - \sigma_y^{th}(p, \dot{p}, T) - R^{th}(p, \dot{p}, T) = 0 \tag{21}$$

where for FCC metals:

$$R^{th}(p, \dot{p}, T) = \hat{R}\left(1 - \left(-\bar{\beta}_2 T \ln\left(\bar{\eta}_0^{vp}\dot{p}\right)\right)^{1/q_1}\right)^{1/q_2} \tag{22}$$

$$\sigma_y^{th} = 0 \tag{23}$$

for BCC metals:

$$R^{th}(p, \dot{p}, T) = 0 \tag{24}$$

$$\sigma_y^{th} = R(p) + Y^{th} \text{ where } Y^{th} = \hat{Y}\left(1 - \left(-\beta_2 T \ln\left(\eta_0^{vp}\dot{p}\right)\right)^{1/q_1}\right)^{1/q_2} \tag{25}$$

Herein Y_a denotes the athermal yield stress, R represent the strain hardening, and Y^{th} and R^{th} are the threshold yield stress and hardening stress at which the dislocations can overcome the barriers without the assistance of thermal activation respectively. Moreover,σ_y^{th} and R^{th} denote the yield stress and hardening as a function of temperature and rate. The constants $0 < q_1 \leqslant 1.0$ and $1.0 < q_1 \leqslant 2.0$ define the shape of the short-range barriers. Their typical values, however, are 3/2 and 2 for the latter that is equivalent to a triangle obstacle profile near the top and 2/3 and 1/2 for the former which characterizes the tail of the obstacle [50]. The material parameter $\beta = k/G_0$ and the viscosity parameter $\eta_0^{vp} = (Mb\rho_i d)^{-1} t_{w0}$ and $\bar{\eta}_0^{vp} = (Mbd(\rho_i d + m(1 - exp(-k_a p))/k_a)^{-1} t_{w0}$ are defined in terms of the microstructure quantities where k is the Boltzmann's constant, G_0 the Gibbs energy at zero Kelvin temperature, M can be interpreted as the Schmidt orientation factor, b is the magnitude of the Burgers vector, d the average distance the dislocation moves between the obstacles, ρ_i the initial dislocation density, m is the multiplication factor and k_a is the dislocation annihilation factor and t_w is the average waiting time of dislocations at an obstacle. The equivalent plastic strain as a function of the indenter depth is then obtained by performing the finite element analysis for the indentation problem using the aforementioned models. In this regard, the proposed viscoplasticity constitutive model is implemented in the commercial finite element program ABAQUS/Explicit (2008) via a user's material subroutine coded as VUMAT including the radial return algorithm.

4. Application of the proposed Model to different metals

In this section the proposed models are investigated in order to capture the behavior of various BCC and FCC metals for different accumulated plastic strains, rates of strain, grain size, distance from the grain boundary, and various temperatures. For BCC metals the results of nanoindentation on single crystal iron [42] at different temperatures, polycrystal tungsten [43] at various strain rates, niobium [44] and iron [13] for different distances from the grain boundary are taken into account. For FCC metals, Single crystal aluminum [15] and polycrystal copper [15] at various strain rates, gold thin film [18] at different temperatures and polycrystal nickel [9] with different grain sizes are considered.

4.1. Iron

BCC iron was chosen as one of the materials for this study because Iron-based alloys are some of the most widely used in structural applications. In order to verify the capability of the proposed physically based model for size effects and length scales at different distances from the grain boundary and various rates of strain, the nanoindentation results reported by Aifantis et al. [13] and Bahr et al. [42] are used respectively. Figure 3(a) compares the proposed TRISE model (Eq.(18)) with the hardness experimental data at different distances from the grain boundary. Increase in hardness as the grain boundary is approached can be seen in this figure which agrees with the prior indentation studies [45-47]. It can be also inferred from this figure that for shorter distances from the grain boundary, the local hardening is successfully captured by the physically based model. For higher distances ($d > 1\mu m$), the hardness decreases with the indentation depth. Since the same parameters are used for macro hardness H_0 (Eq. (20)), all three curves converge to the same value of hardness for higher indentation depths. Making use of Eq. (18) allows one to interpret properly the effect of grain boundary on the hardness. In addition the local hardening effect vanishes for large distances from the grain boundary (i.e. coarse grained size materials).

The material parameters obtained through curve fitting are then used along with Eq.(10) to obtain the material intrinsic length scale shown in Figure 3(b) with reference to the equivalent plastic strain (p). It can be seen from this figure that the intrinsic material length scale decreases from an initial value at yield (this value can be obtained following the procedure proposed by Voyiadjis and Abu Al-Rub [48], regarding the constant length scale) to a final value of $\ell \to 0$ for very high values of accumulated plastic strains (corresponding to the classical, local plasticity limit).

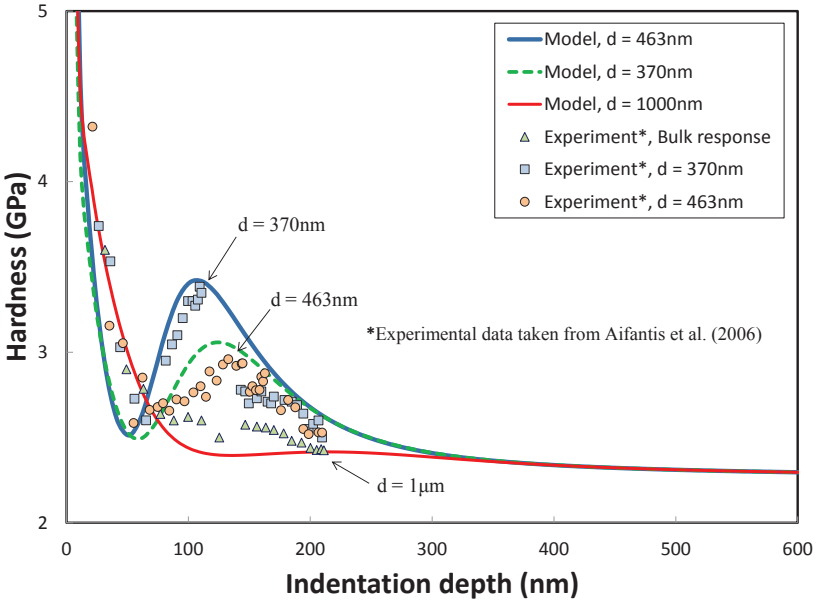

(a)

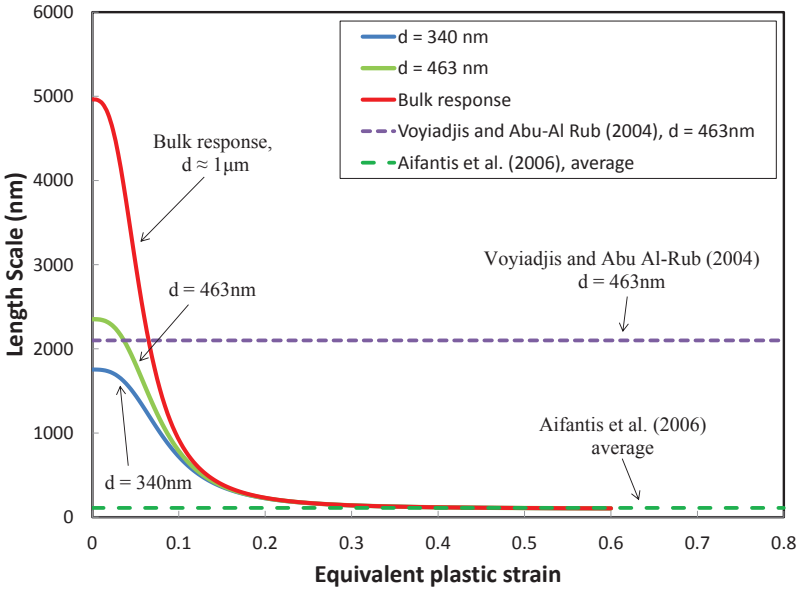

(b)

Fig. 3: (a) Comparison of the proposed model with the experimental results of iron at various distances from the grain boundary (experimental data taken from Aifantis et al. [13]); (b) Material Length Scale versus Equivalent Plastic Strain for iron using the Physically Based Model (Eq. (12)).

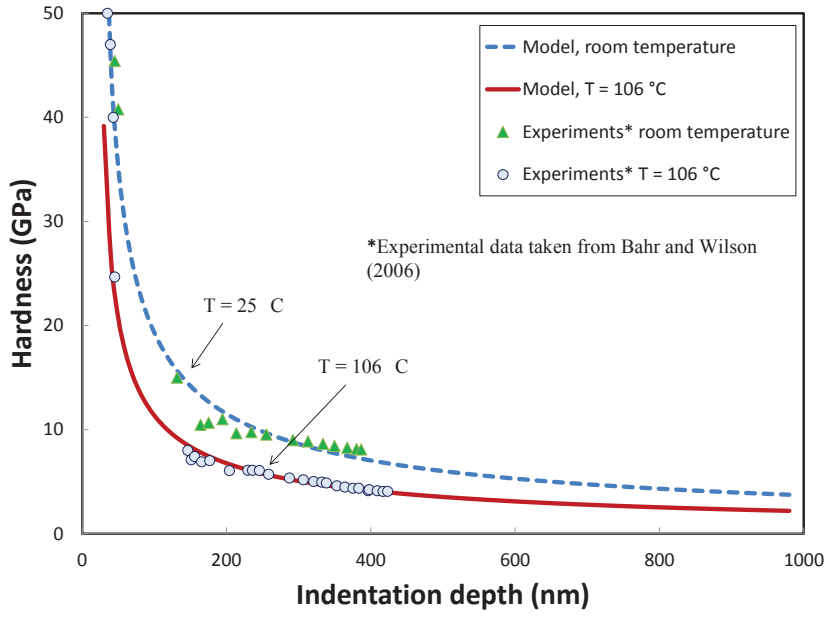

(a)

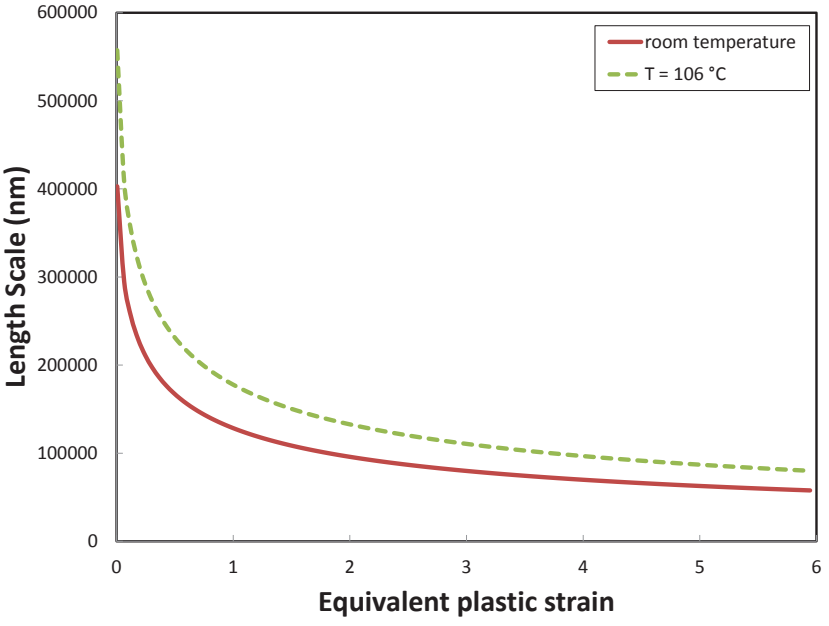

(b)

Fig. 4: (a) Comparison of the proposed model with the experimental results for Fe-3%Si at various temperatures (experimental data taken from Bahr et al. [42]); (b) Material Length Scale versus Equivalent Plastic Strain for iron using the Physically Based Model for single crystal metals (Eq.(9)).

The values of constant length scale obtained from Voyiadjis and Abu Al-Rub approach and reported by Aifantis et al. [13] using the current experimental data are also shown in this figure. Moreover, it can be inferred that the difference in grain size affects the value of the length scale obtained from Eq. (11) for lower plastic strains. In the case of higher strains the value of the length scale is the same for various grain sizes.

Bahr et al. [42] performed nanoindentation experiments on Fe-3%Si single crystal for different temperatures at the strain rate of 5 nm/s. The results of hardness as a function of indentation depth are shown in Figure 4(a) as well as the curves obtained from the physically based model for single crystal metals. It can be seen from the experimental results that the assumption of grain boundary mechanism for hardening/softening effect is justified, as it does not occur in single crystals. This figure also shows that both experiments and proposed physically based models for TRISE (Eq. (16)) and macro hardness show the decrease in hardness with increase in temperature. The calibrated material constants δ_1,δ_2,and δ_3 are used to obtain the variable material length scale for the single crystal iron. The variation of the intrinsic material length scale with equivalent plastic strain (p) is shown in Figure 4(b). It is observed that higher temperature results in higher length scales.

4.2. Nickel

In this section, the results of nanoindentation on nickel with different grain sizes performed by Yang and Vehoff [9] are used in order to measure the material constants of the proposed TRISE model. The nanoindentation was conducted in the center of the individual grains on an NC nickel plate of high purity ($> 99.97\%$) and very low porosity with grains of approximate diameter $80\mu m$, $1350nm$ and $850nm$. In order to compare the proposed TRISE model with the hardness curves of nickel, first the h^* vs d relation needs to be obtained. Based on the value of from the experiments on nickel with 1350nm and 850nm grain sizes ($h^* = 23nm$ and $h^* = 9.51nm$ respectively), the corresponding $\delta_5 = 12.146$ and $\delta_6 = 160.28$ are evaluated from Eq.(19). In this regard the value for h^* for nickel with $80\mu m$ of grain size is $h^* = 18500nm$. Figure 5 (a) shows the comparison of the Physically-based model with the nano hardness experiments provided by Yang and Vehoff [9]. It can be seen from this figure that for smaller grain sizes, the local hardening is successfully captured by the physically based model. In the coarse grain size ($d = 80\mu m$), the hardness decreases with the indentation depth. It is also inferred from this figure that the proposed model provides a good description of the TRISE for different grain sizes. Furthermore, with inclusion of the grain boundary effect, it is able to capture the hardening/softening effect for smaller grain sizes. Using the assumed value for the Nye factor ($\bar{r} = 1.9$), the material length scale can be obtained using the Physically-based expression of the length scale (Eq. (10)) for the polycrystalline nickel as shown in Figure 5 (b) with reference to the equivalent plastic strain (p). It can be seen from this figure that the intrinsic material length scale decreases from an initial value at yield to a final value of $\ell \rightarrow 0$ for very high values of accumulated plastic strains corresponding to the classical, local plasticity limit. Moreover, it can be inferred that the difference in grain size affects the value of the length scale obtained from Eq.(10) for lower plastic strains while for the higher strains, the value of the length scale is the same for various grain sizes.

4.3. Single crystal aluminum

Nano-hardness experiments conducted on single crystal aluminum at various strain rates by Voyiadjis et al. [15] are used here to examine the validity of the proposed formulation for single crystal materials under different strain rates. Finite element analysis is performed for different strain rates using the physically based constitutive model for FCC metals in order to obtain values for the $p(h)$. The accumulated plastic strain contours obtained from this analysis is shown in Figure 6(a). The TRISE model for single crystal (Eq. (22)) is then compared with the nano-indentation experiments. Figure 6(b) shows the comparisons of hardness with reference to indentation depth at $0.05/s$ and $0.1/s$ of strain rate. It can be inferred from the experimental results that the assumption of grain boundary mechanism for hardening/softening effect is justified, as it does not occur in single crystals. The insignificant hardening effect for the single-crystal aluminum subjected to $0.1/s$ strain rate can be interpreted as a small vacancy that affects the results. Comparisons between the experimental data and simulations in Figure 6 show that the proposed model of TRISE for single-crystal materials and macro hardness H_0 both agree well with the response of the metals at various strain rates. The material intrinsic length scale obtained from the calibrated parameters is presented in Figure 7 . It can be seen from this figure that the length scale decreases as the plastic strain increases.

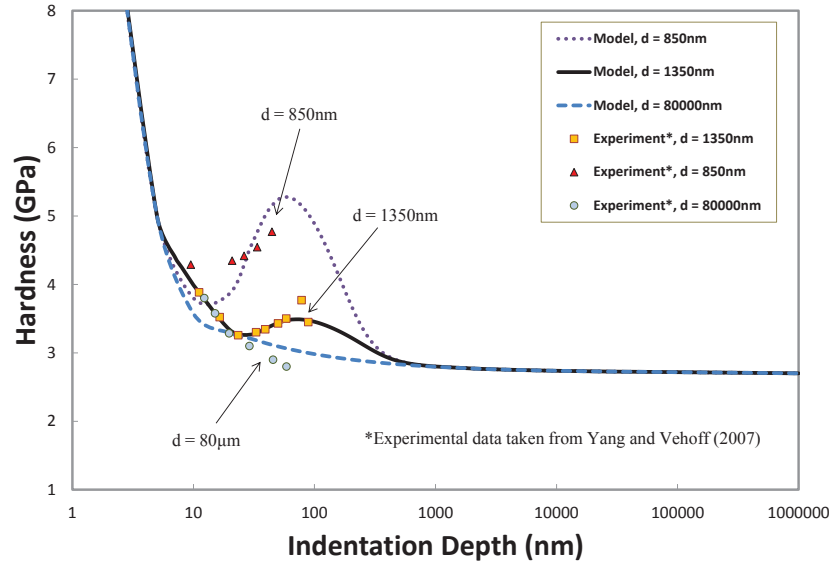

(a)

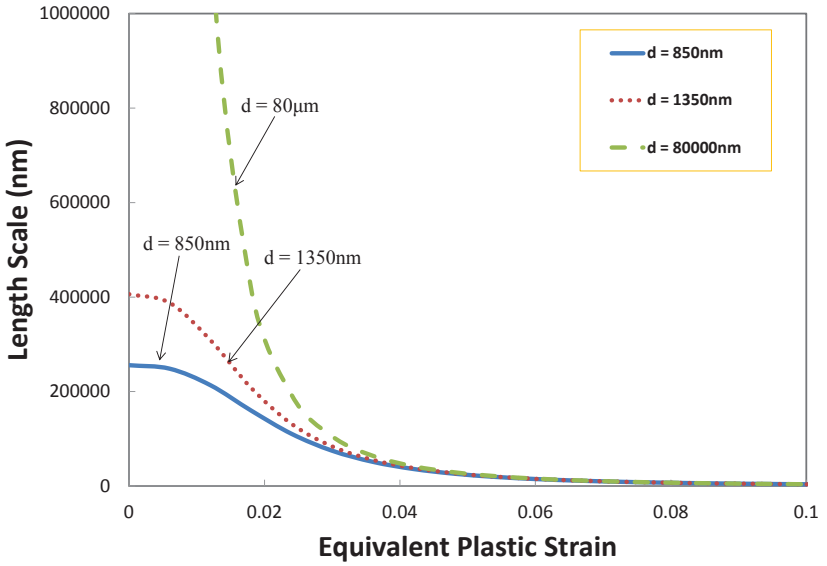

(b)

Fig. 5: (a) Comparison of the proposed model with the experimental results for nickel at various grain sizes (experimental data taken from Yang and Vehoff [9]); (b) Material Length Scale versus Equivalent Plastic Strain for Polycrystalline Nickel using the Physically Based Model (Eq. (10)).

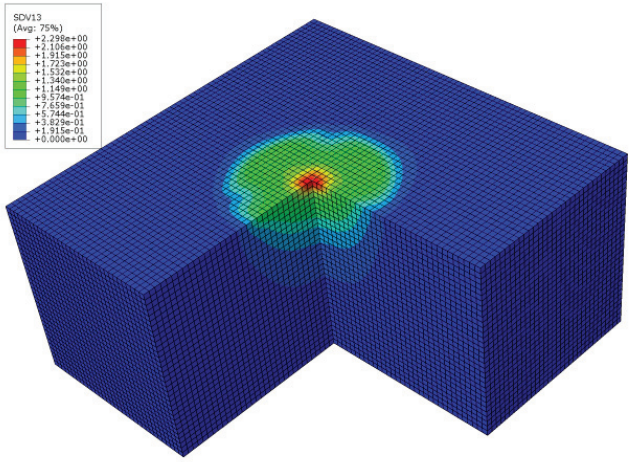

(a)

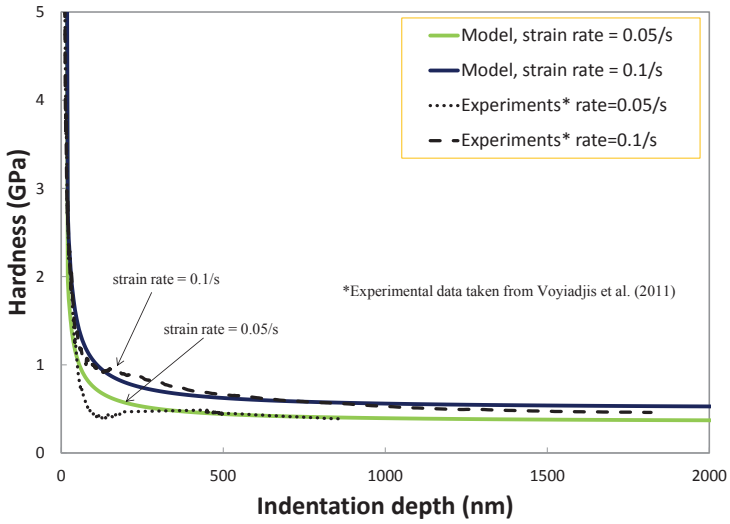

(b)

Fig. 6: Finite element results of nanoindentation problem for Aluminum (b) Comparison of the proposed model with the experimental results for single crystal aluminum at different strain rates (experimental data taken from Voyiadjis et al. [15]).

4.4. Niobium

Niobium is a BCC metal with a melting point of $2741K$ that is used as an alloying agent in carbon and alloy steels and in non-ferrous metals, as it improves the strength of the alloy. Wang and Ngan [44] conducted a sequence of nanoindentation tests on cylindrical specimens with a $6.35mm$ diameter and $5mm$ length of niobium with 99.99% purity made by an electronbeam melting method. These specimens were then annealed for 20 days at a temperature of 1200 °C in a vacuum of approximately 10^{-5} Torr, followed by furnace cooling to room temperature. The resultant grain size was $500 \pm 200\mu m$. To reveal the grain boundary, the samples were etched in an etchant containing $60ml$ HF (48% concentration), $40ml H_2O_2$ (30% concentration), and $0.55g$NaF, for about $10 - 20s$. A Berkovich indenter was used for making indents along selected grain boundaries on the Nb sample. Since grains with sectional dimensions of larger than $300\mu m$ were always selected for indentation, and the Berkovich indenter is in fact a very blunt indenter

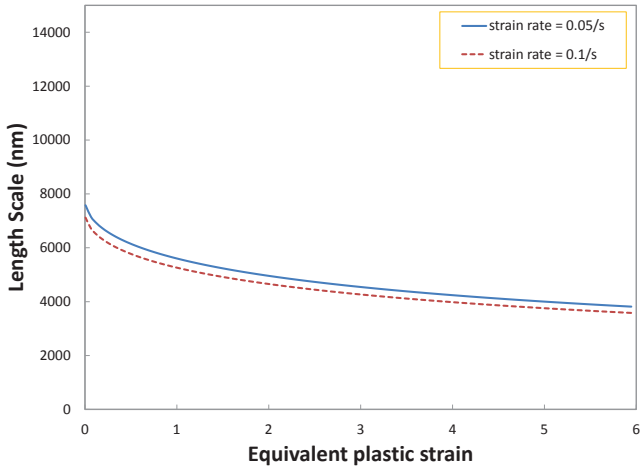

Fig. 7: Material Length Scale versus Equivalent Plastic Strain for single crystal aluminum using the Physically Based Model (Eq. (9))

with an apex angle of 140.6, the grain boundaries were highly unlikely to develop sharp curvatures within a depth of only about $1\mu m$ below the surface and to be intersected by the indenter below the surface. The backscattered SEM images from the performed indentation near the grain boundary are presented in Figure 8. In this figure, the regions with brighter contrast encircled by dotted lines near the grain boundary show the extent of lattice rotation around the indents. Wang and Ngan [44] indicated that pop-in in the load-penetration curve is observed in Figure 8 (c) but not in Figure 8 (d). This indicates that the two grain boundary segments have very different potential to transmit slip.

Nano-hardness experiments results at the distance of $3.82\mu m$ and $6.81\mu m$ from grain boundary are used here to examine the validity of the proposed formulation for niobium. An extensive approach to obtain the different material constants needed for the proposed micro-structural based constitutive model is presented here.True stress-strain curves of niobium at temperatures ranging from 77 to 800 K and for various strain rates (0.001-8000/s) obtained by Nemat-Nasser and Guo [49] are used in this case. Material parameters are obtained through a three step procedure. The first step is to acquire the initial threshold stress Y_a. This is done by plotting the change in yield stress with the change in temperature. The yield stress decreases with increasing temperature up to a point where it becomes almost constant, which is the initial threshold stress,Y_a. The next step is to use a stress-strain curve at a temperature higher than 650 K (where there is no thermal stress) in order to determine the plastic strain related parameters. According to Kocks [50], the typical values of the exponent q_1 are $3/2$ and 2 that is equivalent to the triangle obstacle profile near the top of the obstacle profile for the flow stress. On the other hand, the typical values of the exponent q_2 are less than 1 and it is chosen here to be $1/2$ which characterizes the tail of the obstacle. Once these exponents are determined for a particular mechanism, they are used as material constants.

The $p(h)$ results obtained from the conducted Finite element analysis by means of the aforementioned parameters for the constitutive model is used in the TRISE model for polycrystallines to compare with the nanoindentation experiments provided by Wang and Ngan [44]. As previously mentioned, the parameter d in the equation is assumed to be equal to the distance between indenter and the grain boundary. Figure 9 shows the comparisons of hardness with reference to indentation depth at the distance of $3.82\mu m$ and $6.81\mu m$ from the grain boundary. Comparisons of the experimental data and simulations in Figure 9 (a) show that the proposed models of TRISE for polycrystalline materials and macro hardness H_0 agree well with the response of the metals at various distances from the grain boundary. The material intrinsic length scales obtained using the calibrated parameters are presented in Figure 9 (b).

4.5. Tungsten

Tungsten is a steel-gray BCC metal that is used by forging, drawing, extruding or sintering. Of all the metals in pure form, tungsten has the highest melting point ($3422^{\circ}C$), the lowest vapor pressure, and (at temperatures above

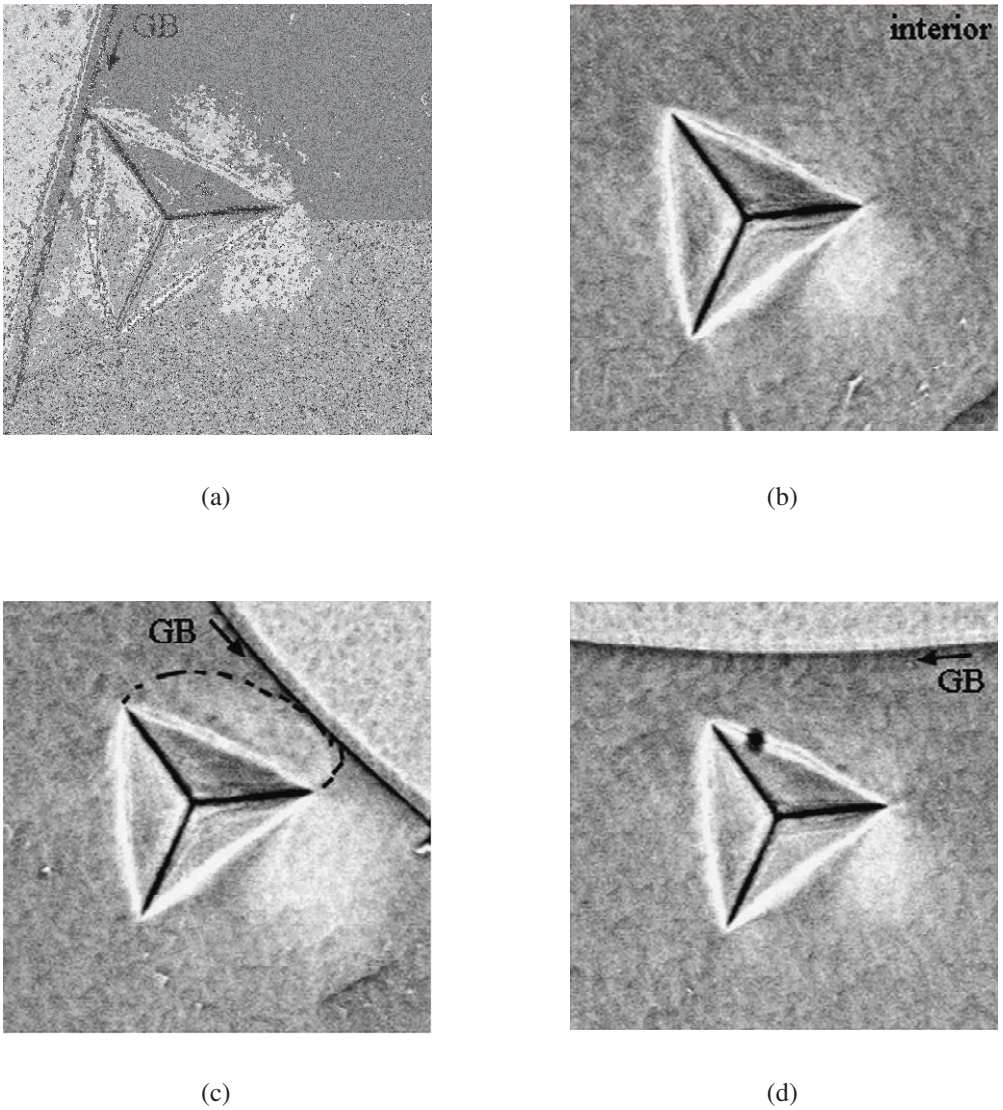

Fig. 8: Backscattered SEM images of indents made using a load of 50mN: (a) indent showing grain-boundary hardening near a grain boundary, (b) an indent within grain interior showing no hardening/softening, (c) an indent showing local hardening, and (d) an indent near a grain boundary but not showing grain-boundary hardening [44].

$1,650^{\circ}C$) the highest tensile strength. The low thermal expansion and high melting point and strength of tungsten are due to strong covalent bonds formed between tungsten atoms by the $5d$ electrons [51]. Alloying small quantities of tungsten with steel greatly increases its toughness. Tungsten is mainly used in the production of hard materials based on tungsten carbide, one of the hardest carbides, with a melting point of $2770^{\circ}C$. WC is an efficient electrical conductor, but W2C is less therefore WC is used to make wear-resistant abrasives and cutters and knives for drills, circular saws, milling and turning tools used by the metalworking, woodworking, mining, petroleum and construction industries [51]. Tungsten's high melting point makes tungsten a good material for applications like rocket nozzles, for example in the UGM-27 Polaris Submarine-launched ballistic missile [52]. Superalloys containing tungsten, such as Hastelloy and Stellite, are used in turbine blades and wear-resistant parts and coatings. Vadalakonda, et al. [43]

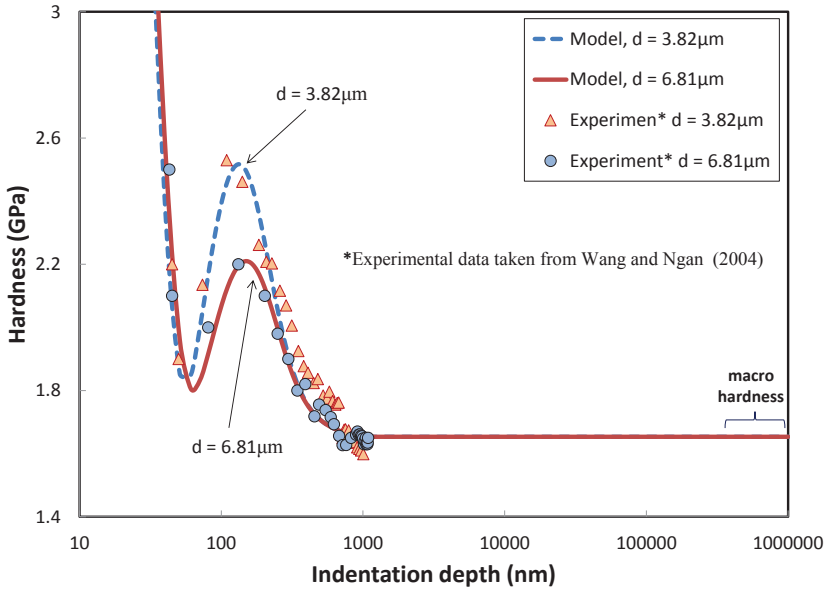

(a)

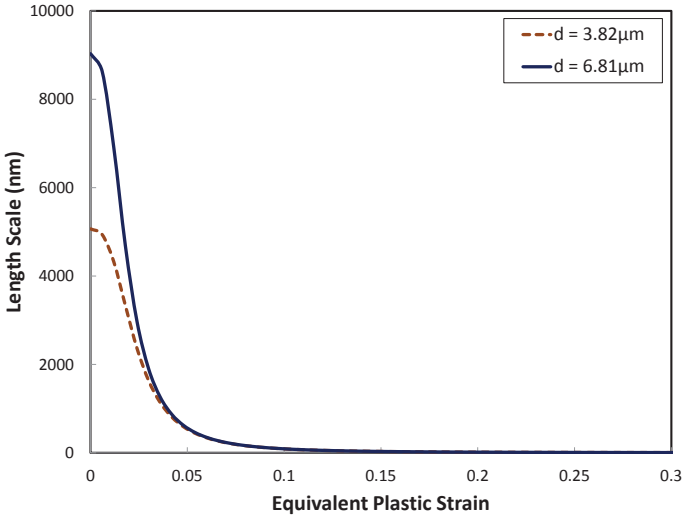

(b)

Fig. 9: (a) Comparison of the proposed model with the experimental results for Niobium at various distances from the grain boundary (experimental data taken from Wang and Ngan [44]); (b) Material Length Scale versus Equivalent Plastic Strain for Polycrystalline Niobium using the Physically Based Model (Eq.(10)).

provided load-displacement curves of nanoindentation tests on polycrystalline tungsten in various strain rates. The samples were foils with 1.5*mm* thickness, < 99.9% purity, and grain sizes of 6μm. These samples were mechanically polished and the nanoindentation experiments were carried out in an MTS Nanoindeter XP instrument. The reason

for polishing is to reduce the friction effect of the surface and indenter in the obtained results. On the other hand, the density of dislocations will be affected by polishing and if the density is higher, the amount of dislocations in the pileup required to generate the critical shear stress will be reached earlier during the loading cycle [13]. Tests were conducted with different strain rates, ranging from $0.003 - 0.1/s$ in the displacement control mode using the XP Basic Hardness, Modulus method (standard method prescribed for the Nanoindenter XP instrument).

The experimental results using the Berkovich indenter are used in this section to verify the capability of the proposed physically based model for size effects and length scales at various rates of strain. These experiments are performed at $0.003/s$, $0.01/s$, and $0.1/s$ of strain rate and at room temperature. Standard method proposed by Oliver and Pharr [53] is used in order to determine the hardness-indentation depth curves from the provided load-depth. In order to obtain the equivalent plastic strain as a function of indentation depth, $p(h)$, the constitutive model parameters of Tungsten reported by Wei et al. [54] and Dummer et al. [55] are taken into account. By obtaining the $p(h)$ from the finite element analysis and H_0 from the physically based equation, one is able to compare the developed TRISE model with the experimental data. Figure 11 (a) compares the proposed model with the hardness experimental data in the case of Tungsten. The macro readings are obtained discretely at millimeter scale, in contrast to the results of indentations obtained by the nanoindenter, which mostly start at about $7 - 10nm$ up to a few micrometers. Increase in hardness due to increase in strain rate can be also seen in Figure 11 (a). Moreover, Strong hardening/softening effects are noticed from the experimental results. The experimental data for hardness versus depth at 0.1/s of strain rate are also shown in this figure. From the comparison of the model with the experiments in Figure 11(a), it can be concluded that the proposed model is adequate in describing the TRISE for different low strain rates. Furthermore, it is able to capture the local hardening even when a strong hardening/softening effect is exhibited. It is also observed in this figure that the physically based model for predicting the macro hardness proposed in the previous section gives relatively accurate predictions of H_0 at different strain rates. The physically based model parameters used in obtaining H_0. The material parameters obtained through curve fitting in Figure 11(a) are used along with Eq. (10) in order to obtain the material intrinsic length scale, which is shown in Figure 11(b). As indicated in Figure 11(b), the length scale increases with an increase in the strain rate.

4.6. Copper

The nano-indentation experiments on copper conducted by Voyiadjis et al. [15] for different strain rates are used in this section in order to verify the capability of the proposed physics based model for size effects and length scales at various rates of strain. These experiments are performed at $0.05/s$, $0.08/s$, and $0.1/s$ strain rates and at room temperature. Voyiadjis et al. [15] indicated that the equipment is not able to capture the hardening/softening effect at higher rate of strains due to the lack of data points reported by the instruments. They also performed additional experiments on single crystal material in order to check the validity of the concept assumed here for local hardening in nanoindentation.

In order to obtain the equivalent plastic strain as a function of indentation depth, $p(h)$, the constitutive model parameters of copper reported by Voyiadjis and Abed [40] are taken into account. By obtaining the $p(h)$ from the finite element analysis using the aforementioned micromechanical based constitutive model for FCC metals and H_0 from the physically based equation, one is able to compare the developed TRISE with the experimental data. Figure 11(a) compares the proposed model with the hardness experimental data in the case of copper. The macro readings are obtained discretely at millimeter scale, in contrast to the results of indentations obtained by the nanoindenter, which mostly start at about $7 - 10nm$ up to few micrometers. Increase in hardness due to increase in strain rate can be also seen in Figure 4. Moreover, strong hardening/softening effect is noticed from the experimental results, which agree well with the observations of other researchers [11, 14]. It should be noted that the experimental data are smoothed in order to determine the material parameters. The experimental data for hardness versus depth at $0.1/s$ of strain rate are also shown in this figure. The local hardening in this case is not as clear as for the other curves. One may conclude that for this device there is a lower strain rate limit that can capture the hardening/softening effect. From the comparison of the model with the experiments in Figure 4, it can be concluded that the proposed model is adequate in describing the TRISE for different low strain rates. Furthermore, it is able to capture the local hardening even when a strong hardening/softening effect is exhibited. It is also observed that the physics-based model for predicting the macro hardness proposed in the previous section gives relatively accurate predictions of H_0 at different strain rates. The material parameters obtained through curve fitting in Figure 11 (a) are used along with Eq. (10) in order to obtain the material intrinsic length scale which is shown in Figure 11 (b).

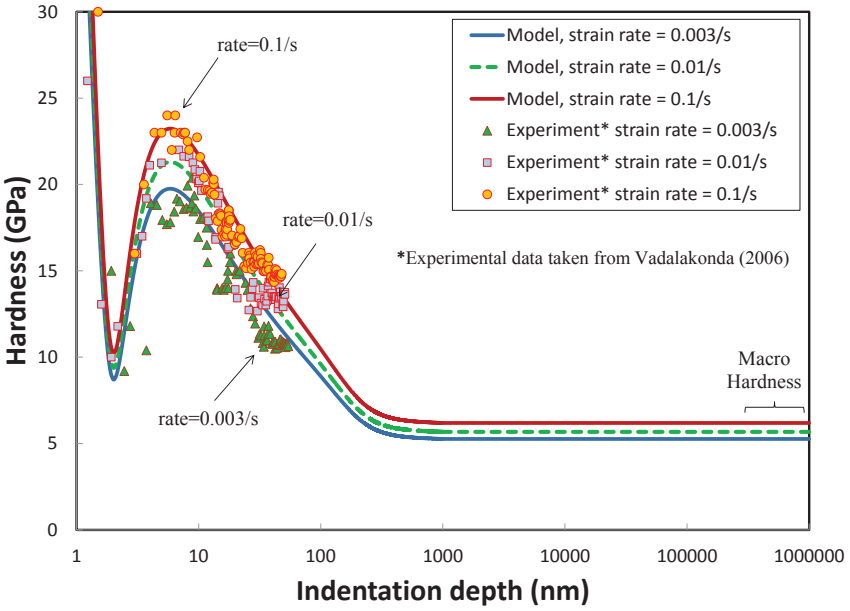

(a)

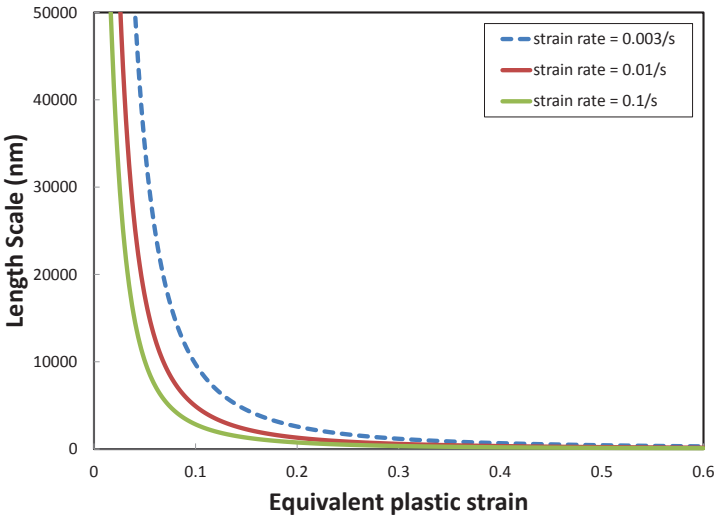

(b)

Fig. 10: (a) Comparison of the proposed model with the experimental results for Tungsten at various strain rates (experimental data taken from [43]). (b)Material Length Scale versus Equivalent Plastic Strain for Polycrystalline Tungsten using the Physically Based Model (Eq.(10))

4.7. Gold thin film

Volinski, et al. [18] performed high temperature nano-hardness experiments using a local heating approach on $2.7\mu m$ gold film sputter-deposited onto polished $< 100 >$ silicon substrate. A series of increasing temperature indentations were conducted followed by room temperature experiments. Since both load-depth curves performed at room

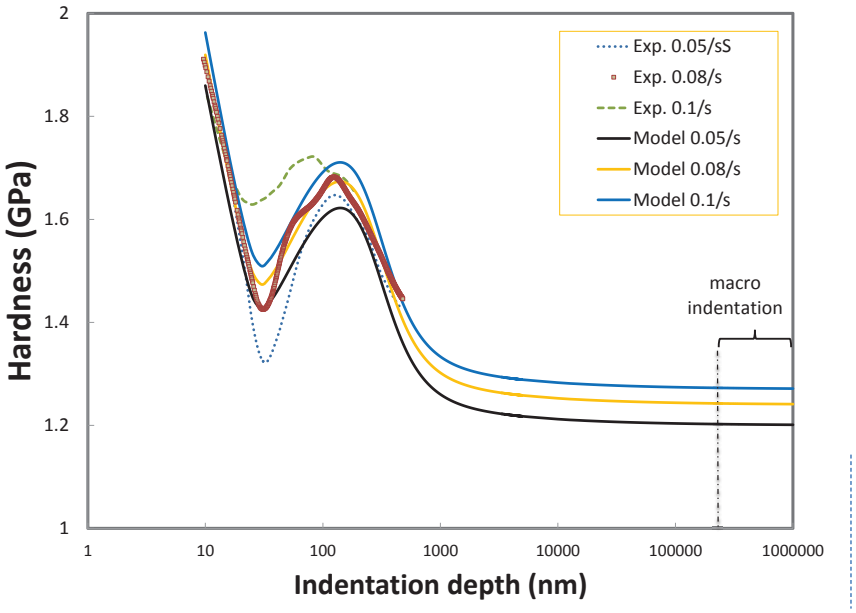

(a)

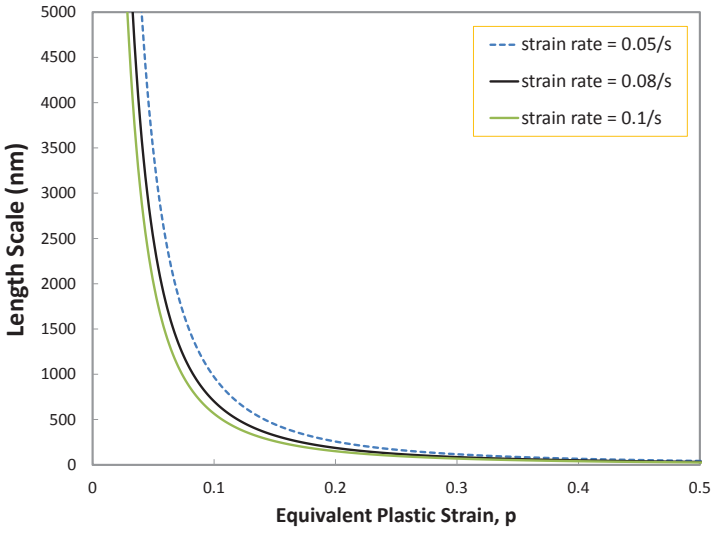

(b)

Fig. 11: (a) Comparison of the proposed model with the experimental results of Copper at various temperatures (experimental data taken from Voyiadjis et al. [15]); (b) Material Length Scale versus Equivalent Plastic Strain for Copper using the Physically Based Model (Eq. (10)).

temperature before and after heating were identical, one can ensure that there were no annealing effects. The temperature effect is more pronounced for the nanocrystalline and also it shows more strength compared to the bulk material. In order to determine the constitutive model (for FCC metals) parameters used in the finite element simulation of the indentation test, the yield stress-temperature curves obtained by Volinski, et al. [18] for the thin film as well as the

stress-strain curves of the gold micro wire at different strain rates [56] are used. This allows one to obtain the values of $p(h)$ that are closer to the real behavior of the thin film gold.

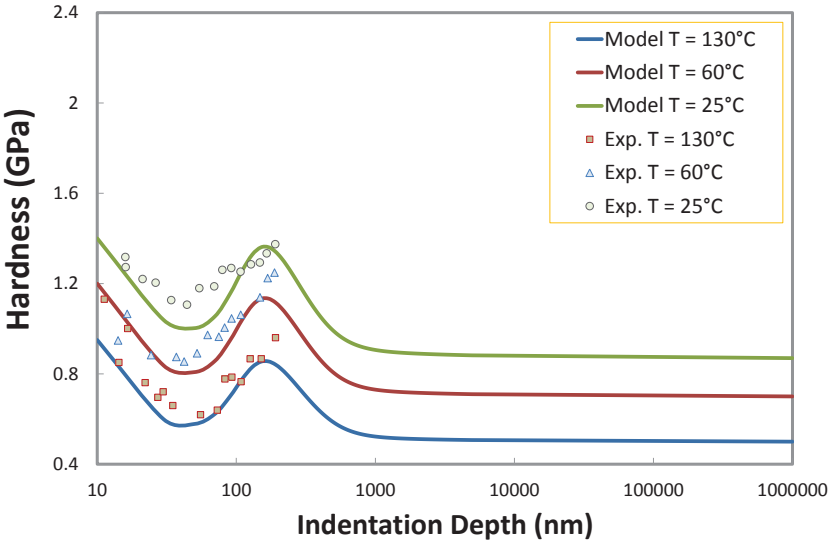

(a)

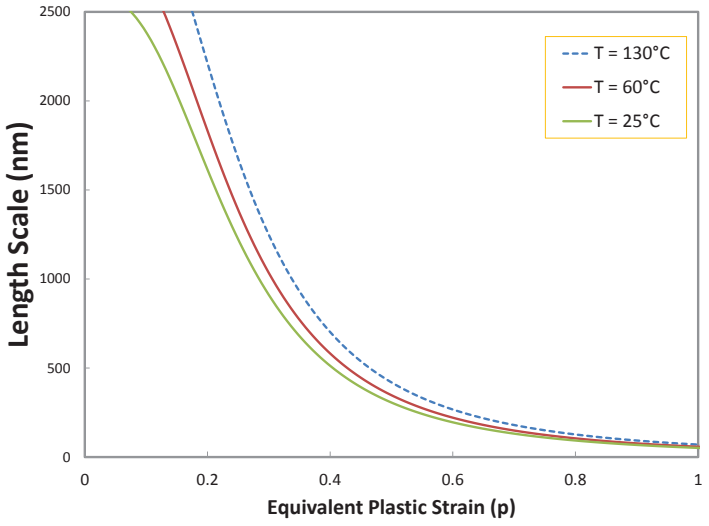

(b)

Fig. 12: (a)Comparison of the proposed model with the experimental results for Gold at various temperatures (experimental data taken from Volinsky, et al. [18]);(b) Material Length Scale versus Equivalent Plastic Strain for thin film Gold using the physically based Model (Eq. (10)).

The results of hardness as a function of indentation depth, as well as the curves obtained from the physically based model, are shown in Figure 12(a). Volinski, et al. [18] indicated that the effect of substrate became apparent at

about 200*nm* of indentation depth, and therefore the experimental data points after this depth are not considered in the curve fitting process in Figure 12. Also, the value of 200*nm* is also used as the grain size in the proposed expressions of TRISE and length scale. It can be inferred from this figure that both experiments and proposed physically based models for TRISE and macro hardness show a decrease in hardness with increase in temperature. The physically based model parameters are used in obtaining H_0. The calibrated material constants δ_1, δ_2 , and δ_3 are used to obtain the variable material length scale for the thin film gold. The variation of the intrinsic material length scale with equivalent plastic strain (p) is shown in Figure 12(b). It is observed that higher temperatures result in higher length scales.

5. Conclusion

Through the use of gradient plasticity, the behavior of the microstructure is incorporated into the classical continuum theory in order to address problems involving strain localizations and instabilities. As the associated local deformation gradients become sufficiently large in comparison with the characteristic dimension of the system, one needs to introduce these refined continuum theories with their associated length scales. It follows that experiments are needed to quantify such length scales. Such experiments may be difficult to design and interpret. The work presented here provides an extensive effort in calibration of the strain gradient plasticity theory and size effects. Physically based models to predict simultaneously the Temperature and Rate Indentation Size Effect (TRISE) and length scale from nanoindentation experiments are proposed here for both single and polycrystalline materials. This model is based on the evolution of geometrically necessary dislocations (GNDs) beneath the indenter which is nonlinearly coupled to the evolution of statistically stored dislocations (SSDs) through the Taylor hardening law. The hardening/softening effect observed in polycrystalline materials is included in the model by involving the effect of grain boundaries as barriers to the spreading of the plastic zone. In general, there are three factors contributing to the resistance to slip transfer leading to local hardening: (i) Geometric condition: the angle between the lines of interaction of the incoming and outgoing slip planes with the grain boundary; (ii) Resolved shear stress condition; and (iii) Residual grain boundary dislocation condition. The Burgers vector of the residual dislocation is determined from the difference between the Burgers vectors of incoming and outgoing dislocations [57]. The higher magnitude of the Burgers vector of this residual dislocation leads to a stronger hardening/softening effect. This and the resolved shear stress condition determine the active slip direction. The aforementioned factors which are supported by both experimental and theoretical studies [58-60] are considered in the proposed TRISE model through contributing the material constants. Moreover, based on the aforementioned theory, a relation between grain size (or distance from grain boundary in course grained metals) (d) and the indentation depth regarding to initiation of the local hardening (h^*) is obtained. The nanoindentation experiments on the various FCC and BCC metals are used to evaluate the capability of the proposed model for different low strain rates. The equivalent plastic strain is determined using the finite element simulation for the nanoindentation problem along with a microstructural physically based viscoplastic (rate and temperature dependent) constitutive model implemented into ABAQUS/Explicit (2008) as a user subroutine in VUMAT. It is worth noting that making use of a gradient dependent material model results in more accurate results. However, as it is explained before, the strain gradient is included in the formulation through the GNDs evolution under the indenter and in order to account for rate and temperature effects the proposed temperature and rate dependent constitutive model is considered. Furthermore, the micromechanical based model based on the behavior of dislocation densities developed by Almasri and Voyiadjis [38] is used to acquire the macro hardness for different strain rates. The proposed framework is then investigated using experimental results in order to capture the behavior of the materials for different accumulated plastic strains, rates of strain, distance from the grain boundary, and various temperatures. Comparison of the experimental results and the proposed models show that one can capture the TRISE at different strain rates, temperatures, and various grain sizes. In addition, it can be concluded that the effect of the grain boundaries play the major role in the hardening/softening effect since no major local hardening effect is captured in the single crystal materials, as previously discussed by Voyiadjis et al. [15]. Also, combining the relation between the grain size and h^* with the TRISE model for polycrystalline metals leads to the vanishing of the hardening/softening effect for coarse grain sizes (i.e. larger distances between indenter and the grain boundary) in this model. Material length scales for the tested materials at different strain rates, distance from grain boundary and elevated temperatures are determined. The physically based model is calibrated using the nanoindentation test. This model is defined in terms of the Nye factor (characterizes the microstructure dimension), Schmidt's orientation factor (characterizes the lattice rotation), the Burgers vector (characterizes the displacement carried out by each dislocation), and the empirical constant α (characterizes the deviation

from regular spatial arrangement of the SSDs or GNDs population). The proposed physically based model introduces strain rate and temperature dependency in a coupled form through the expression of the average distance between SSDs. The obtained length scales from this model vary with the accumulated plastic strain, strain rate, temperature and grain size (or distance from grain boundary). The proposed physically based model gives good predictions for the length scales in both single- and polycrystalline materials. These models are used within a wide range of accumulated plastic strains. The proposed length scale is shown to decrease significantly with the accumulated plastic strain. At high strains the length scale tends to zero, corresponding to the local plasticity theory. It is noted also that the length scale increases with the increase in temperature and grain size (distance from grain boundary) and decreases with the increase in strain rate. In general, it can be concluded that the harder materials have smaller values of length scales, since materials with smaller length scales require greater loads in order to create the same contact area, which states that the additional amount of hardening during deformation increases as ℓ increases. Therefore, the indentation size effect is expected to be affected by both prior dislocations and additional work hardening that takes place during indentation. Also, it has been shown that in small amounts of equivalent plastic strain, higher distances from grain boundaries lead to higher values of the length scale. However, when the plastic strain increases, the length scale for various distances merges to the same value. This indicates that the effect of the grain boundary is only prominent in the first stage of loading, where the boundary can obstruct the movement of GNDs. After overcoming this barrier, the length scale will be the same at higher plastic strains.

Acknowledgments

The first author acknowledges the collaboration with Professor Taehyo Park of the Hanyang University, Seoul, Korea, under the World Class University project funded by the National Research Foundation of Korea.

References

[1] Abu Al-Rub, R.K. and G.Z. Voyiadjis, *Analytical and experimental determination of the material intrinsic length scale of strain gradient plasticity theory from micro- and nano-indentation experiments*, International Journal of Plasticity, Cambridge Univ. Press, Cambridge, 2004. 20(6): p. 1139–1182.

[2] Fleck, N.A. and J.R. Willis, *A mathematical basis for strain-gradient plasticity theory-Part I: Scalar plastic multiplier*. Journal of the Mechanics and Physics of Solids, 2009. 57(1): p. 161-177.

[3] Voyiadjis, G.Z. and B. Deliktas, *Formulation of strain gradient plasticity with interface energy in a consistent thermodynamic framework.* International Journal of Plasticity, 2009. 25(10): p. 1997-2024.

[4] Gurtin, M.E. and L. Anand, *Thermodynamics applied to gradient theories involving the accumulated plastic strain: The theories of Aifantis and Fleck and Hutchinson and their generalization.* Journal of the Mechanics and Physics of Solids, 2009. 57(3): p. 405-421.

[5] Begley, M.R. and J.W. Hutchinson, *The mechanics of size-dependent indentation.* Journal of the Mechanics and Physics of Solids, 1998. 46(10): p. 2049-2068.

[6] Soifer, Y.M., A. Verdyan, M. Kazakevich, and E. Rabkin, *Nanohardness of copper in the vicinity of grain boundaries.* Scripta Materialia, 2002. 47(12): p. 799-804.

[7] Soer, W.A. and J.T.M. De Hosson, *Detection of grain-boundary resistance to slip transfer using nanoindentation.* Materials Letters, 2005. 59(24-25): p. 3192-3195.

[8] Delince, M., P.J. Jacques, and T. Pardoen, *Separation of size-dependent strengthening contributions in fine-grained Dual Phase steels by nanoindentation.* Acta Materialia, 2006. 54(12): p. 3395-3404.

[9] Yang, B. and H. Vehoff, *Dependence of nanohardness upon indentation size and grain size - A local examination of the interaction between dislocations and grain boundaries.* Acta Materialia, 2007. 55(3): p. 849-856.

[10] Voyiadjis, G.Z. and A.H. Almasri, *A physically based constitutive model for fee metals with applications to dynamic hardness.* Mechanics of Materials, 2008. 40(6): p. 549-563.

[11] Voyiadjis, G.Z., A.H. Almasri, and T. Park, *Experimental nanoindentation of BCC metals.* Mechanics Research Communications, 2010. 37(3): p. 307-314.

[12] Almasri, A.H. and G.Z. Voyiadjis, *Nano-indentation in FCC metals: experimental study.* Acta Mechanica, 2010. 209(1-2): p. 1-9.

[13] Aifantis, K.E., W.A. Soer, J.T.M. De Hosson, and J.R. Willis, *Interfaces within strain gradient plasticity: Theory and experiments.* Acta Materialia, 2006. 54(19): p. 5077-5085.

[14] Voyiadjis, G.Z. and R. Peters, *Size effects in nanoindentation: an experimental and analytical study*. Acta Mechanica, 2010. 211(1-2): p. 131-153.

[15] Voyiadjis, G.Z., D. Faghihi, and C. Zhang, *Analytical and Experimental detemination of rate, and temperature dependent length scales using nanoindentation experiments*. Journal of Nanomechanics and Micromechanics, ASCE, 2011. 1(1): p. 24-40.

[16] Orowan, E., *Mechanical strength properties and real structure of crystals.* Zeitschrift Fur Kristallographie, 1934. 89(3/4): p. 327-343.

[17] Taylor, G.I., *Plastic strain in metals.* Journal of the Institute of Metals, 1938. 62: p. 307-324.

[18] Volinsky, A.A., N.R. Moody, and W.W. Gerberich, *Nanoindentation of Au and Pt/Cu thin films at elevated temperatures.* Journal of Materials Research, 2004. 19(9): p. 2650-2657.

[19] Fleck, N.A. and J.W. Hutchinson, *Strain gradient plasticity.* Advances in Applied Mechanics, Vol 33, 1997. 33: p. 295-361.
[20] Ashby, M.F., *The deformation of plastically non-homogenous alloys.* Philosophical Magazine 1970. 21: p. 399-424.
[21] Nix, W.D. and H.J. Gao, *Indentation size effects in crystalline materials: A law for strain gradient plasticity.* Journal of the Mechanics and Physics of Solids, 1998. 46(3): p. 411-425.
[22] Columbus, D. and M. Grujicic, *A comparative discrete-dislocation/nonlocal crystal-plasticity analysis of plane-strain mode I fracture.* Materials Science and Engineering a-Structural Materials Properties Microstructure and Processing, 2002. 323(1-2): p. 386-402.
[23] Arsenlis, A. and D.M. Parks, *Crystallographic aspects of geometrically-necessary and statistically-stored dislocation density.* Acta Materialia, 1999. 47(5): p. 1597-1611.
[24] Gao, H., Y. Huang, and W.D. Nix, *Modeling plasticity at the micrometer scale.* Naturwissenschaften, 1999. 86(11): p. 507-515.
[25] Bammann, D.J. and E.C. Aifantis, *On a Proposal for a Continuum with Microstructure.* Acta Mechanica, 1982. 45(1-2): p. 91-121.
[26] Gracio, J.J., *The Double Effect of Grain-Size on the Work-Hardening Behavior of Polycrystalline Copper.* Scripta Metallurgica Et Materialia, 1994. 31(4): p. 487-489.
[27] Faghihi, D. and G.Z. Voyiadjis, *Size effects and length scales in nanoindentation for body-centred cubic materials with application to iron* .Proceedings of the Institution of Mechanical Engineers, Part N: Journal of Nanoengineering and Nanosystems, 2010. 224: p. 5-18.
[28] Faghihi, D. and G.Z. Voyiadjis, *Determination of nanoindentation size effects and variable material intrinsic length scale for body-centered cubic metals.* Mechanics of Materials, 2011. In Press, Corrected Proof.
[29] Voyiadjis, G.Z. and D. Faghihi, *Variable (intrinsic) material length scale for face-centred cubic metals using nano-indentation.* Proceedings of the Institution of Mechanical Engineers, Part N: Journal of Nanoengineering and Nanosystems, 2011.
[30] Voyiadjis, G. and R.K. Abu Al-Rub, *Length Scales in Gradient Plasticity Theory,* in Proceedings of the IUTAM Symposium on Multiscale Modeling and Characterization of Elastic-Inelastic Behavior of Engineering Materials, M.C. S. Ahzi, M. A. Khaleel, H. M. Zbib, M. A. Zikry, and B. LaMatina, Editor. 2002, Kluwer Academic Publishers: Morocco. p. 167-174.
[31] Tabor, D., *The Hardness and Strength of Metals.* Journal of the Institute of Metals, 1951. 79(7): p. 1-18.
[32] Shen, Z., R.H. Wagoner, and W.A.T. Clark, *Dislocation and Grain-Boundary Interactions in Metals.* Acta Metallurgica, 1988. 36(12): p. 3231-3242.
[33] Gemperlova, J., M. Polcarova, A. Gemperle, and N. Zarubova, *Slip transfer across grain boundaries in Fe-Si bicrystals.* Journal of Alloys and Compounds, 2004. 378(1-2): p. 97-101.
[34] Vystavel, T., A. Jacques, A. Gemperle, J. Gemperlova, and A. George, *Dislocation interaction with a Sigma=3 grain boundary observed by in-situ TEM.* Intergranular and Interphase Boundaries in Materials, Iib98, 1999. 294-2: p. 397-400.
[35] Voyiadjis, G.Z. and R.K. Abu Al-Rub, *Thermodynamic based model for the evolution equation of the backstress in cyclic plasticity.* International Journal of Plasticity, 2003. 19(12): p. 2121-2147.
[36] Voyiadjis, G.Z. and I.N. Basuroychowdhury, *A plasticity model for multiaxial cyclic loading and ratchetting.* Acta Mechanica, 1998. 126(1-4): p. 19-35.
[37] Feng, G. and W.D. Nix, *Indentation size effect in MgO.* Scripta Materialia, 2004. 51(6): p. 599-603.
[38] Almasri, A.H. and G.Z. Voyiadjis, *Effect of strain rate on the dynamic hardness in metals.* Journal of Engineering Materials and Technology-Transactions of the Asme, 2007. 129(4): p. 505-512.
[39] Schmidt, E.E. and W. Boas, *Crystal plasticity*. 1950, London: Hughes.
[40] Voyiadjis, G.Z. and F.H. Abed, *Implicit algorithm for finite deformation hypoelastic-viscoplastici in fcc metals.* International Journal for Numerical Methods in Engineering, 2006. 67(7): p. 933-959.
[41] Voyiadjis, G.Z. and F.H. Abed, *A coupled temperature and strain rate dependent yield function for dynamic deformations of bcc metals.* International Journal of Plasticity, 2006. 22(8): p. 1398-1431.
[42] Bahr, D.F., D.E. Wilson, and D.A. Crowson, *Energy considerations regarding yield points during indentation.* Journal of Materials Research, 1999. 14(6): p. 2269-2275.
[43] Vadalakonda, S., R. Banerjee, A. Puthcode, and R. Mirshams, *Comparison of incipient plasticity in bcc and fcc metals studied using nanoindentation.* Material Science and Engineering, 2006. A 426 (1-2): p. 208-213.
[44] Wang, M.G. and A.H.W. Ngan, *Indentation strain burst phenomenon induced by grain boundaries in niobium.* Journal of Materials Research, 2004. 19(8): p. 2478-2486.
[45] Soer, W.A., K.E. Aifantis, and J.T.M. De Hosson, *Incipient plasticity during nanoindentation at grain boundaries in body-centered cubic metals.* Acta Materialia, 2005. 53(17): p. 4665-4676.
[46] Aust, K.T., R.E. Hanneman, P. Niessen, and Westbroo.Jh, *Solute Induced Hardening near Grain Boundaries in Zone Refined Metals.* Acta Metallurgica, 1968. 16(3): p. 291.
[47] Watanabe, T., S. Kitamura, and S. Karashima, *Grain-Boundary Hardening and Segregation in Alpha-Iron-Tin Alloy.* Acta Metallurgica, 1980. 28(4): p. 455-463.
[48] Voyiadjis, G. and R.K. Abu Al-Rub, *Determination of the material intrinsic length scale of gradient plasticity theory.* International Journal for Multiscale Computational Engineering, 2004. 2(3): p. 337-400.
[49] Nemat-Nasser, S. and W.G. Guo, *Flow stress of commercially pure niobium over a broad range of temperatures and strain rates.* Materials Science and Engineering a-Structural Materials Properties Microstructure and Processing, 2000. 284(1-2): p. 202-210.
[50] Kocks, U.F., Realistic *constitutive relations for metal plasticity.* Materials Science and Engineering a-Structural Materials Properties Microstructure and Processing, 2001. 317(1-2): p. 181-187.
[51] Lassner, E.S., Wolf-Dieter, *Tungsten - Properties, Chemistry, Technology of the Element*, Alloys, and Chemical Compounds. 1999, Verlag Springer.
[52] Ramakrishnan, P., *Powder-Metallurgy in a New Light. Journal of Scientific and Industrial Research,* 1986. 45(7-8): p. 372-374.
[53] Oliver, W.C. and G.M. Pharr, *An Improved Technique for Determining Hardness and Elastic-Modulus Using Load and Displacement Sensing Indentation Experiments.* Journal of Materials Research, 1992. 7(6): p. 1564-1583.
[54] Wei, Q., T. Jiao, K.T. Ramesh, E. Ma, L.J. Kecskes, L. Magness, R. Dowding, V.U. Kazykhanov, and R.Z. Valiev, *Mechanical behavior and dynamic failure of high-strength ultrafine grained tungsten under uniaxial compression.* Acta Materialia, 2006. 54(1): p. 77-87.

[55] Dummer, T., J.C. Lasalvia, G. Ravichandran, and M.A. Meyers, *Effect of strain rate on plastic flow and failure in polycrystalline tungsten.* Acta Materialia, 1998. 46(17): p. 6267-6290.
[56] Abdullah, S., M.F.M. Yunoh, H. Kamarudin, and A. Jalar, *Role of strain rate on the micromechanical characterization properties of 4N gold micro wire: micro tensile and nanoindentation.* European Journal of Scientific Research, 2009. 28(1): p. 33-43.
[57] Lee, T.C., I.M. Robertson, and H.K. Birnbaum, *Prediction of Slip Transfer Mechanisms across Grain-Boundaries.* Scripta Metallurgica, 1989. 23(5): p. 799-803.
[58] Clark, W.A.T., R.H. Wagoner, Z.Y. Shen, T.C. Lee, I.M. Robertson, and H.K. Birnbaum, *On the Criteria for Slip Transmission across Interfaces in Polycrystals.* Scripta Metallurgica Et Materialia, 1992. 26(2): p. 203-206.
[59] De Koning, M., R.J. Kurtz, V.V. Bulatov, C.H. Henager, R.G. Hoagland, W. Cai, and M. Nomura, *Modeling of dislocation-grain boundary interactions in FCC metals.* Journal of Nuclear Materials, 2003. 323(2-3): p. 281-289.
[60] Zhang, N. and W. Tong, *An experimental study on grain deformation and interactions in an* $Al - 0.5\%Mg$ *multicrystal.* International Journal of Plasticity, 2004. 20(3): p. 523-542.